Computational Simulation on a Coaxial Substream Powder Feeding Laval Nozzle of Cold Spraying

Guosheng HUANG [1, 2] [*], **Daming GU** [1], **Xiangbo LI** [2], **Lukuo XING** [2]

[1] *School of Science, Harbin Institute of Technology, Harbin, China, 150001*
[2] *Science and Technology on Marine Corrosion and Protection Laboratory, Luoyang Ship Material Research Institute, Qingdao, China, 266101*

In this paper, a substream coaxial powder feeding nozzle was investigated for use in cold spraying. The relationship between nozzle structure and gas flow, the acceleration behavior of copper particles were examined by computational simulation method. Also, one of the nozzle was used to spray copper coating on steel substrate. The simulation results indicate that: the velocity of gas at the center of the nozzle is lower than that of the conventional nozzle. Powders are well restrained near the central line of the nozzle, no collision occurred between the nozzle wall and the powders. This type of nozzle with expansion 3.25 can successfully deposit copper coating on steel substrate, the copper coating has low porosity about 3.1 % – 3.8 % and high bonding strength about 23.5 MPa – 26.8 MPa.

Keywords: cold spray, computational simulation, Laval Nozzle.

1. INTRODUCTION

Cold spray, also called cold gas dynamic spray, or kinetic spray, was found by Papyrin in 1980s occasionally in a wind-tunnel experiment. They found that a micron metal particle will adhere to substrate when the particle exceeds a certain velocity [1] named critical velocity. It is a bulk solid coating deposition process which is totally different from conventional thermal spray methods [2]. Cold spray coating is oxidation free and low porosity due to its relative low temperature and high kinetic energy which arouses numerous interests in industrial application.

The impacting velocity is the most important factor which determines particles to deposit or not. In cold spray, a metal particle will deposit onto substrate when the particle exceeds critical velocity [1]. The velocity of the metal particles is complicated determined by the gas inlet temperature, gas inlet pressure, gas type, the geometry structure of Laval nozzle, and characteristics of gas flow inside and outside the nozzle [2]. The most important factor in these parameters is the structure of the nozzle. There are a numerous studies on the gas flow of nozzle and data on the performance of nozzle [3 – 9]. In summary, there are two types of nozzle, one is upstream coaxial powder feeding type, and the other is substream vertical axis feeding type. For upstream coaxial powder feeding type, choking phenomenon are frequently occurring during spraying soft material or in an elevated temperature. For substream vertical feeding type, worn out of nozzle can easily occur after a short period operation. It has great benefit to design a nozzle, which can inherit the advantages of both nozzles. There are some researches on how to optimize nozzle structure for using in a limitation space [10]. There are also numerous data on the gas solid

two phase flow optimization on cold spray nozzle design. But there are now little data reported on the downstream coaxial powder feeding nozzle [11].

In this paper, a downstream coaxial powder feeding nozzle was investigated by FLUENT software based on the gas dynamics. And the acceleration was examined by computational simulation method. One of the nozzle is verified by spraying copper coating.

2. EXPERIMENTAL METHODS

2.1. Structure of coaxial powder feeding laval nozzle

The basic structure of the nozzle is shown in Fig. 1. The exit of powder feeding pipe located at the diverging part of the nozzle. To realize an adjustable mass flow rate in the powder feeding pipe, the position of the exit is placed at different location from nozzle throat to maximum cross-section area surface. According to the gas dynamics, the relationship between the exit Mach number and the expansion ratio can be written as equation (1), in which M stands for Mach numbers of gas, γ is specific heat ratio, A is the area of throat of nozzle and A^e is the area of nozzle exit. The corresponding relationship is shown in Fig. 2. It can be seen from Fig. 2 that there are two Mach numbers corresponding to one expansion ratio. One is subsonic and another is supersonic, this is determined by the pressure ratio between pre-chamber and the atmosphere around the nozzle exit [12]. If the pressure exceeds the critical value, then a supersonic flow occurs after the nozzle throat. The expansion ratio can be written as equation (3), R_1 stands for the diameter of powder feeding pipe at the nozzle throat, R_2 stands for the diameter of nozzle throat, R_3 stands for the diameter of exit of powder feeding pipe, R_4 stands for the maximum cross-section of nozzle. To reduce the gas consumption, the area of nozzle throat must be as small as possible, so it requires a complicated calibration

---

[*]Corresponding author. Tel.: +8613969623961, fax: +8653268725001.
E-mail address: *huanggs@sunrui.net* (G. Huang)

method to manufacture the nozzle. The mass flow rate (m) in the nozzle can be written as equation (2). The length of elongated part (barrel part) of the nozzle can be adjusted as needed, this part also can be a separated one because of the low pressure at this part. The expansion ratios investigated are listed in Table 1.
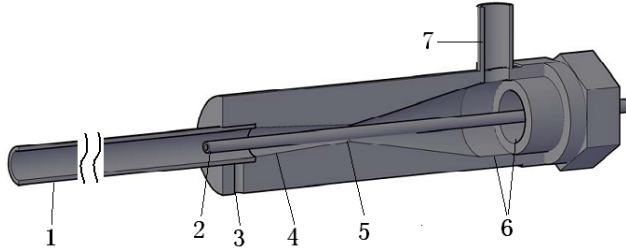

Fig. 1. The basic structure of coaxial substream powder feeding nozzle (1 – elongated tube, 2 – powder feeding pipe, 3 – drill fast, 4 – diverging part, 5 – nozzle throat, 6 – pre-chamber, 7 – carrier gas inlet)

Table 1. Nozzle structures to be investigated for expansion ratio

No.	ER	R_1	R_2	R_3	R_4	L_1	L_2	L_3
1	1.96	3	4	1.5	4	20	15	120
2	3.25	3	4	1.5	5	20	15	120
3	4.82	3	4	1.5	6	20	15	120
4	6.68	3	4	1.5	7	20	15	120

$$\frac{A}{A^e} = \frac{1}{M}\left[\left(\frac{2}{\gamma+1}\right)\left(1+\left(\frac{\gamma-1}{2}\right)M^2\right)\right]^{\frac{\gamma+1}{2(\gamma-1)}}. \tag{1}$$

$$m = A_t \sqrt{\frac{\gamma}{R}\left(\frac{2}{\gamma-1}\right)^{\frac{\gamma+1}{\gamma-1}}} \frac{P_0}{\sqrt{T_0}}. \tag{2}$$

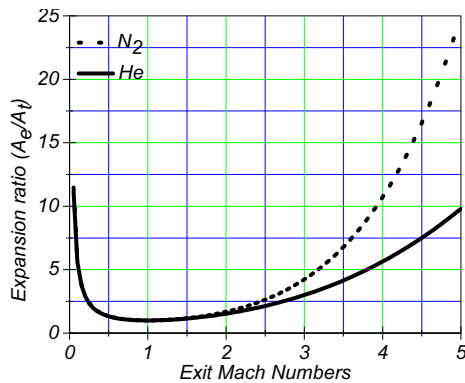$$A_e \Big/ A_t = \frac{R_4^2 - R_3^2}{R_2^2 - R_1^2}. \tag{3}$$

Fig. 2. Relationship between maximum Mach number and expansion ratio for De-Laval-Nozzle (the expansion ratio equals to area of exit surface divided by cross-section area of throat)

2.2. Numerical simulation methods

Numerical modeling was performed using a commercial software FLUENT12 (ANSYS company, US) to determine the flow field of driving gas inside the nozzle and the free jet area, and subsequently the accelerating behavior of particles in cold spraying. A two dimensional axisymmetric model was used as shown in Fig. 3. The length barrel part of the nozzle is 120 mm to guarantee a full development of gas flow. The distance from nozzle to the substrate is fitted as 20 mm. Wall boundary is stationary and adiabatic. The meshing was conducted with the quad elements as shown in Fig. 4. The first mesh scale is 0.01 mm, increment ratio is 1.05 for boundary layer, the total numbers of boundary is 5. All wall boundaries are set as Escape type except substrate, the substrate is set as Trap type. The calculation result independency to mesh density is checked with the $y+(5\sim60)$ [10, 11]. Compressed air is used as processing gas. The gas was taken as an ideal and compressible one, the C_p (specific heat at constant pressure) is 1006.43 J/kg.K, the molecular mass is 28.966. A realizable k-ε model was used to solving the turbulent flow. The detailed realizable k-ε model can be found elsewhere [8 – 10]. The gas parameter in pre-chamber varies from 0.8 MPa – 2.5 MPa, and 473 K to 773 K. The exit location was also examined.
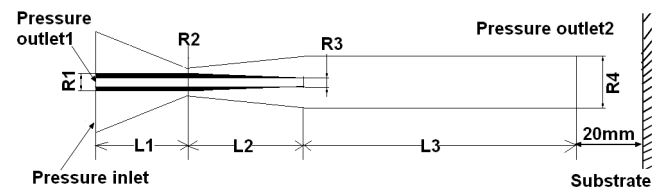

Fig. 3. The computational domain of coaxial substream powder feeding nozzle and its boundary conditions
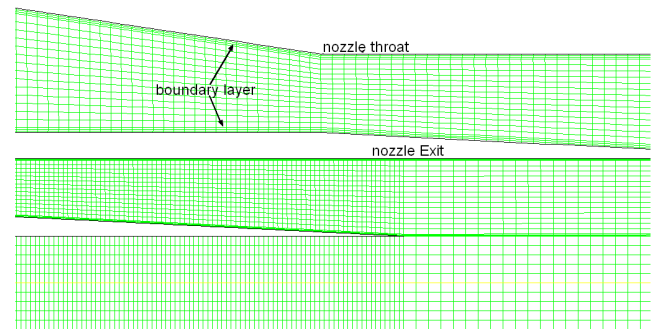

Fig. 4. Schematic diagram of quad meshing strategy for computational domain around the converging-diverging part

Copper particles are used in this simulation with density of 8.9 g/cm³, the molecular mass is 64 g/mol, the particle diameter is set as $2\sim20\,\mu m$ and considered as quasi-spherical ball for all situations. The particles are injected from the pressure-outlet 2, the initial velocity of all particles is set as 5 m/s in the +X direction. The particles acceleration behavior by compressed air can be solved by equation (4) and equation (5) using the model proposed by Morsi and Alexander [11, 12] when the particles are considered as quasi-spherical, dilute phase as the particles loading rate is 1 g/s. It is assumed that heat conduction within a particle is neglected and the particle is therefore treated as isothermal. F_x is the correlation terms including "effective mass": force, pressure gradient induced force and thermophoretic force. Gravity acceleration is expressed as g_x. In this study, the F_x and g_x can be regarded as 0. The drag coefficient correlation equations are different for supersonic and subsonic flow. The drag coefficient correlation can be written as

equation (6). And the drag coefficient can finally be written as equation (7) simplified by [13], and coefficient is listed in Table 2.

$$\frac{du_p}{dt} = F_D(u - u_p) + g_x(\rho_p - \rho)/\rho_p + F_x .$$ (4)

$$\text{Re}_p = \rho_g d_p \left| \frac{u_p - u_g}{u_g} \right| .$$ (5)

$$F_D = \frac{18p}{\rho_p d_p^2} \frac{C_D \text{Re}}{24} .$$ (6)

$$C_c = a_1 + \frac{a_2}{\text{Re}_p} + \frac{a_3}{\text{Re}_p} .$$ (7)

D_p is the diameter of particle, F_D is the drag coefficient, C_c is the Stokes drag Cunningham correlation. u is velocity of the gas flow, ρ is the gas density, ρ_p is the particles density.

Table 2. Drag force coefficient [11]

Re	a_1	a_2	a_3
Re<0.1	0	24.0	0
0.1<Re<1.0	3.69	22.73	0.0903
1.0<Re<10.0	1.222	29.1667	−3.8889
10.0<Re<100.0	0.6167	46.5	−116.67
100.0<Re<1000.0	0.3644	98.33	−2778
1000.0<Re<5000.0	0.357	148.62	−4.75×10^5
5000.0<Re<10000.0	0.46	−490.456	57.87×10^4
10000.0<Re<50000.0	0.5191	−1662.5	5.4167×10^5

2.3. Verification of simulation results

The experiment is conducted to verify whether this kind of nozzle can be used to deposit coatings or not. Nozzle No. 2 was used to spray coating, the expansion ratio is 3.25. Q235 steel (3 mm) was used as substrate, abraded with emery paper of number 280 and 600 in sequence. Copper alumina mixed powder was used to form coating. The nominal content of alumina is about 40 % in volume. The morphology of the powder is shown in Fig. 5.
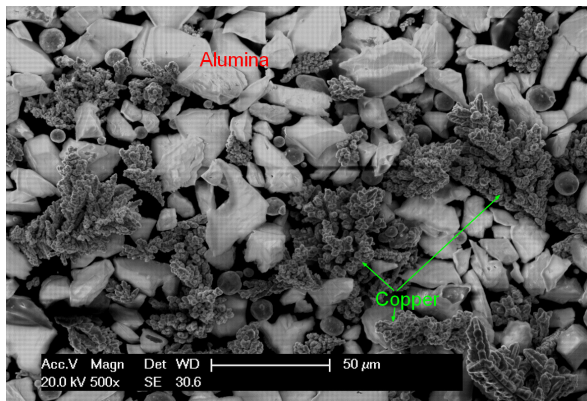

Fig. 5. ESEM morphology of mixed copper alumina powder used for depositing coating

The size of most copper powders ranges from 5 μm to 20 μm, the shape of the powder is acerose. A very small part of the copper is spherical. Most of the particles are agglomerated with several small particles. The gas parameter in the prechamber is 1.6 MPa and 673 K. The powder was fed at the exit of the Laval nozzle through syphonage, the powder feed rate is controlled by moving rate of the other end of the powder feeder pipe. Compressed air was adopted as carrier gas. The transverse speed of spray gun is 5 cm/s. The distance between nozzle exit to the substrate is about 25 mm.

3. RESULTS

3.1. Characteristics of gas flow in laval nozzle

The gas flow of different pressure and temperature in prechamber is shown in Fig. 6 and Fig. 7. It can be seen from Fig. 6 that gas reaches to maximum velocity as it arrives to the maximum area, then decreases as it travels through the barrel part. Higher pressure in prechamber, slower the velocity of gas decreases.
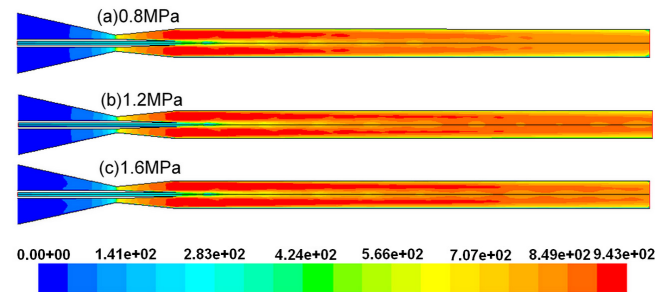

Fig. 6. The contour of gas velocity in the nozzle under temperature of 673 K and different inlet pressure (expansion ratio 3.25)
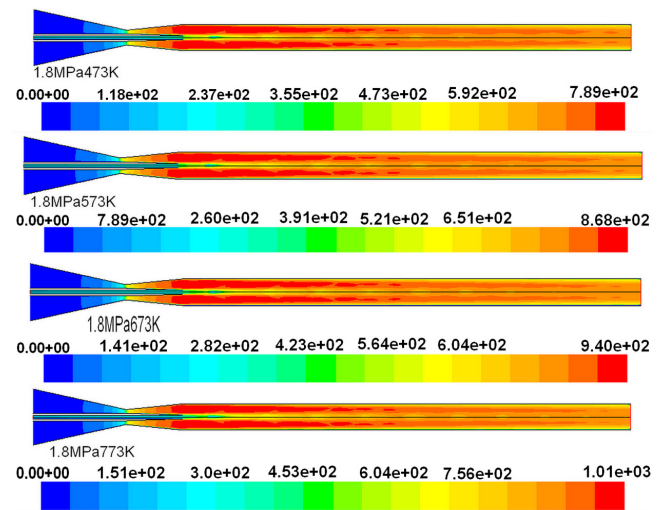

Fig. 7. The contour of gas velocity in the nozzle under different inlet temperature and inlet pressure of 1.8 MPa (Expansion ratio 3.25)

With different gas temperature and pressure in prechamber, the mass flow rate in the powder feeding pipe varies from (2.74 ~ 2.77) kg/s as shown in Fig. 8. It can be seen that the gas temperature and the gas pressure in prechamber has little effect on the mass flow rate in powder feeding pipe. The pressure of the gas at the powder feeding exit reaches to minimum as the gas velocity

reaches to its highest value, so the pressure difference between atmosphere and the pressure at the exit varies little with the variation of parameter in prechamber. Situation is the same for the gas velocity in the powder feeding pipe, the velocity varies from 220 m/s to 250 m/s. Temperature in prechamber has little effect on the gas flow in the nozzle under the same pressure. Unlike the conventional nozzle, the highest velocity area distribute near the nozzle wall. The gas syphonaged into the nozzle mixes with the main supersonic gas, and decelerates the supersonic gas to a lower speed. But the temperature in prechamber will change the sonic velocity, so the highest velocity is different with each inlet temperature. Obviously, the maximum gas velocity at the center of the nozzle is about 120 m/s lower than the highest velocity around the nozzle wall in this case.
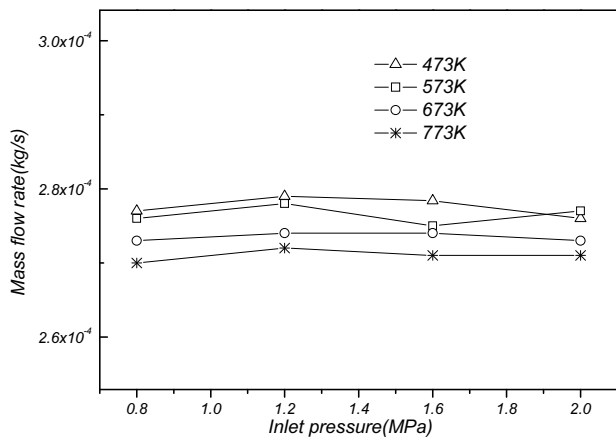

Fig. 8. The mass flow rate in powder feeding pipe influenced by inlet pressure and temperature (Expansion ratio 3.25)
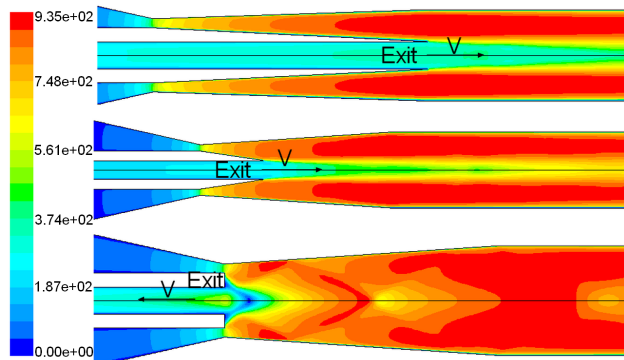

Fig. 9. Effect of the exit location of powder feeding pipe on the gas flow of nozzle under the pressure 1.6 MPa and temperature 673 K in prechamber

The gas flow of nozzle with different powder exit location is shown in Fig. 9. Apparently, the nozzle with a powder feeding exit at the throat has a good gas develop in the nozzle barrel part, but the gas travels at an inverse direction with the main gas flow in powder feeding pip. According to previous study, powder feeding pressure must be about 0.1 MPa – 0.2 MPa higher than the main gas pressure if the powder exit located at the converging part. While the powder exit located at the throat, the pressure at this site is critical pressure, is always higher than atmosphere pressure. The gas pressure decreases abruptly to minimum value as it reaches to a certain location at the

diverging part. At the diverging part, the mass flow rate in the powder feeding pipe can be adjusted by the location of exit as shown in Fig. 10. The velocity in the powder feeding pipe is also influenced by the location. Apparently, the nozzle has no use in this application because additional powder feeder is needed.
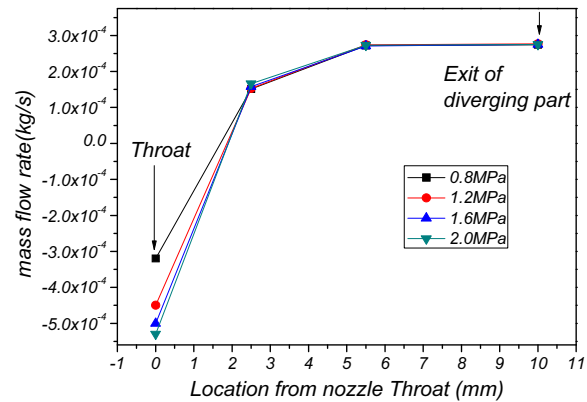

Fig. 10. The mass flow rate in powder feeding pipe influenced by exit location (Inlet pressure1.6 MPa, inlet temperature 673 K and expansion ratio 3.25)

3.2. influence of expansion ratio on the gas flow

Gas flow in the nozzle of different expansion ratio is shown in Fig. 11. Maximum velocity of gas at the exit is influenced by the expansion ratio. The gas flow in the powder feeding pipe is also influenced by the expansion ratio. When the expansion ratio is 1.96, the gas travels in an inverse direction with the main gas flow. This means that the gas is can not be drawn into the nozzle through the powder feeding pipe.
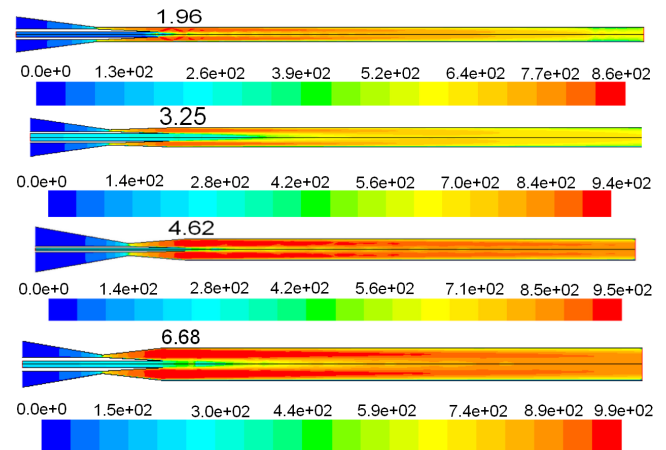

Fig. 11. The contour of gas velocity in the nozzle under temperature of 673 K and inlet pressure 1.6 MPa

The expansion ratio has little effect on the mass flow rate in the powder feeding pipe while the expansion ratio is larger than 4.5. The mass flow rate in the powder feeding pipe is about 5×10^{-5} kg/s when the expansion ratio is 1.96 as shown in Fig. 12. This means that a small part of gas will blew out from it. This will also lower down the gas energy in the substream. This phenomenon occurs mainly due to the structure, the gas compelling out by the high pressure in this place.
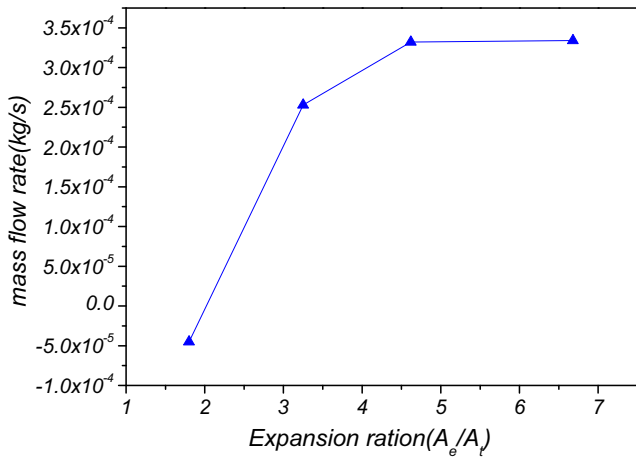
Fig. 12. The mass flow rate in powder feeding pipe influenced by expansion ratio under 1.6 MPa and 673 K

3.3. Acceleration behavior of particle in the nozzle

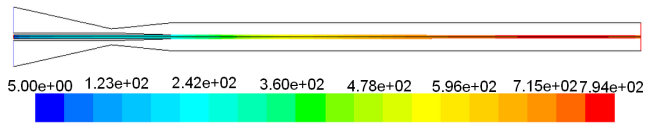A typical trajectory of copper particle in the nozzle is shown in Fig. 13.

Fig. 13. Particle (5 μm copper) trajectories in the nozzle under the pressure of 1.2 MPa and temperature 673 K in pre-chamber

It can be seen that the width of the particle stream is about 2 mm, and well defined around the axis. The spray band is much smaller than conventional upstream powder feeding nozzle. It is worth noting that all particles are assumed to be injected in X direction. Actually, the particles have a random injection direction at the Pressure Outlet1 [14, 15]. As in conventional nozzle, most of the particles always travel through the highest gas velocity area in the nozzle. While in coaxial nozzle, the highest velocity area of gas is around the nozzle wall, the the particle always travels through the central of the nozzle. The gas density is also different, so the acceleration behavior is also different. It can be expected that the particle will have a lower exit velocity than conventional nozzle under the same operation parameters. The maximum particle velocity in powder feeding pipe is about 160 m/s for 2 μm copper particles under this situation and varies little as the inlet pressure and temperature varies. Particle varies little under other situation except expansion ratio 1.96.

Acceleration behavior of different diameter particles is shown in Fig. 14. The pressure and temperature influenced on particle exit velocity are shown in Fig. 15. The particles exit velocity decreases as the diameter increases under the same situation. But it can be seen that most of the particles exceeds the critical velocity (437 ±47) m/s measured by F. Raletz [2]. Such a large deviation of measured value mainly contributes to surface oxidation on the particle surface, which was discussed by W.Y. Li [16].
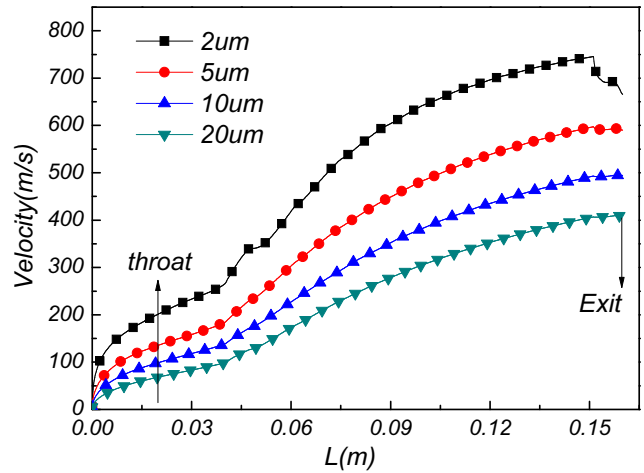

Fig. 14. Particle acceleration behavior along axis the under the pressure of 1.2 MPa and temperature 673 K
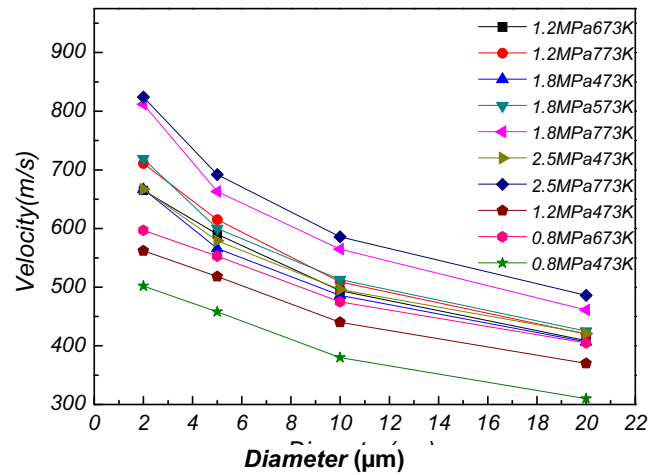

Fig. 15. Particle acceleration behavior along the axial under the expansion ratio of 3.25

3.4. Characteristics of copper alumina coating prepared by nozzle No. 2

Macro morphology of Cu+Al$_2$O$_3$ coating prepared by nozzle No. 2 is shown in Fig. 16.

Fig. 16. Macro morphology of Cu+Al$_2$O$_3$ coating prepared by nozzle No. 2

The characteristics of Cu+Al$_2$O$_3$ coating is listed in Table 3. The deposition efficiency of copper Cu+Al$_2$O$_3$ is roughly calculated and is about 62.5 %. The bonding strength of the coating is about 23.5 MPa – 26.8 MPa. The porosity is about 3.1 % – 3.8 %. The No. 2 nozzle can be used to spray copper coating.

Table 3. The characteristics of Cu+Al$_2$O$_3$ coating

No.	Bonding strength, MPa	Porosity, %	DE, %	Thickness, μm
1	23.5	3.6		
2	26.8	3.1	~62.5	500~800
3	25.5	38.0		

Above results indicate that coaxial substream powder feeding Laval nozzle can be used for cold spray and can successfully deposit Cu+Al$_2$O$_3$ coating on steel substrate. The mass flow rate of gas in powder feeding pipe can be adjusted by selecting the exit location. This syphonage effect can significantly simplify the structure of cold spray system because high pressure powder feeder is not needed. The powder can be drawn into the nozzle be syphonage effect while the expansion ratio is larger than 1.96. According to equation (2) and equation (3), this nozzle consumes about 1.75 times about the conventional nozzle with a 2 mm throat diameter.

4. CONCLUSIONS

Based on the results of this paper the following conclusions can be drawn. The velocity of gas at the center of the nozzle is lower than that of the conventional nozzle. Powders are well restrained near the central line of the nozzle, no collision occurred between the nozzle and the powders. This type of nozzle with expansion 3.25 can successfully deposit copper coating on steel substrate, the copper coating has low porosity about 3.1 % – 3.8 % and high bonding strength 23.5 MPa – 26.8 MPa.

REFERENCES

1. **Alkhimov, A. P.,   Papyrin, A. N.,   Kosarev, V. F., Nesterovich, N. J., Shuspanov, M. M.** Gas-Dynamic Spray Method for Applying a Coating. U. S. Patent 5.302.414. April1 2, 1994.

2. **Raletz, F., Vardell, M., Ezo'o, G.** Critical Particle Velocity under Cold Spray Conditions   *Surface & Coatings Technology* 201 2006: pp. 1942 – 1947.

3. **Spencer, K., Zhang, M.** Optimisation of Stainless Steel Cold Spray Coatings Using Mixed Particle Size Distributions *Surface & Coatings Technology* 205 2011: pp. 5135 – 5140.

4. **Papyrin, A. N.,   Alkhimov, A. P.,   Kosarev, V. F.** Cold Spray Technology [M]. Elsevier, The Netherland, 2007: pp. 178 – 188.

5. **Jen, T. C. , Pan, L. M., Li, L. J., Chen, Q. H., Cui, W. Z.** The Acceleration of Charged Nano-particles in Gas Stream of Supersonic De-Lavel-type Nozzle Coupled with Static Electric Field *Applied Thermal Engineering* 27 2007: pp. 2877 – 2887.

6. **Li, G., Wang, X. F., Li, W. Y.** Effect of Different Incidence Angles on Bonding Performance in Cold Spraying *Transactions of Nonferrous Metals Society of China*   17 2007: pp. 116 – 121. http://dx.doi.org/10.1016/S1003-6326(07)60058-2

7. **Binder, K., Gottschalk, J., Kollenda, M., Gartner, F., Klassen, T.** Influence of Impact Angle and Gas Temperature on Mechanical Properties of Titanium Cold Spray Deposits *Journal of Thermal Spray Technology* 20 (1 – 2) 2011: pp. 234 – 242.

8. **Li, S., Muddle, B., Jahedi, M.** A Numerical Investigation of the Cold Spray Process Using Underexpanded and Overexpanded Jets *Journal of Thermal Spray Technology* doi: 10.1007/s11666-011-9691-4.

9. **Lee, M. W., Park, J. J., Kim, D. Y.** Numerical Studies on the Effects of Stagnation Pressure and Temperature on Supersonic Flow Characteristics in Cold Spray Applications *Journal of Thermal Spray Technology*   20 (5)   2011: pp. 1081 – 1094.

10. **Li, W. Y., Liao, H. L., Douchy, G., Coddet, C.** Optimal Design of a Cold Spray Nozzle by Numerical Analysis of Particle Velocity and Experimental Validation with 316L Stainless Steel Powder *Materials and Design* 28 2007: pp. 2129 – 2137. http://dx.doi.org/10.1016/j.matdes.2006.05.016

11. **Li, W. Y., Liao, H. L., Wang, H. T., Li, C. J., Zhang, G., Coddet, C.** Optimal Design of a Convergent-barrel Cold Spray Nozzle by Numerical Method   *Applied Surface Science* 253 2006: pp. 708 – 716.

12. **Schmidt, T.,   Gartner, F.,   Assadi, H.,   Kreye, H.** Development of a Generalized Parameter Window for Cold Spray Deposition *Acta Materialia* 54 2006: pp. 729 – 742.

13. **Jodoin, B., Raletz, F., Vardelle, M.** Cold Spray Modeling and Validation Using an Optical Diagnostic Method *Surface Coating Technology* 200 2006: pp. 4424 – 4432.

14. **Lupoi, R., O'Neill, W.** Powder Stream Characteristics in Cold Spray Nozzles   *Surface and Coatings Technology* 206 2011: pp. 1069 – 1076. http://dx.doi.org/10.1016/j.surfcoat.2011.07.061

15. **Ghelichi, R., Bagherifard, S., Guagliano, M., Verani, M.** Numerical Simulation of Cold Spray Coating *Surface & Coatings Technology* 23 (205) 2011: pp. 5294 – 5301.

16. **Li, W. Y., Liao, H. L., Li, C. J., Bang, H. S., Coddet, C.** Numerical Simulation of Deformation Behaviour of Al Particles Impacting on Al Substrate and Effect of Surface Oxide Films on Interfacial Bonding in Cold Spraying *Applied Surface Science* 253 2007: pp. 5084 – 5091.